Received: 20 October 2022 | Accepted: 27 February 2023

DOI: 10.1111/1365-2745.14094

Journal of Ecology | BRITISH ECOLOGICAL SOCIETY

RESEARCH ARTICLE

Climate, soil mineralogy and mycorrhizal fungi influence soil organic matter fractions in eastern US temperate forests

Ashley K. Lang[1] | Jennifer Pett-Ridge[2,3] | Karis J. McFarlane[4] | Richard P. Phillips[1]

[1]Department of Biology, Indiana University, Bloomington, Indiana, USA

[2]Physical and Life Sciences Directorate, Lawrence Livermore National Laboratory, Livermore, California, USA

[3]Life and Environmental Sciences Department, University of California Merced, Merced, California, USA

[4]Center for Accelerator Mass Spectrometry, Lawrence Livermore National Laboratory, Livermore, California, USA

Correspondence
Ashley K. Lang
Email: al40@iu.edu

Funding information
Department of Energy, Grant/Award Number: DE-AC52-07NA27344; National Science Foundation, Grant/Award Number: 2010724

Handling Editor: Zeqing Ma

Abstract

1. Identifying the primary controls of particulate (POM) and mineral-associated organic matter (MAOM) content in soils is critical for determining future stocks of soil carbon (C) and nitrogen (N) across the globe. However, drivers of these soil organic matter fractions are likely to vary among ecosystems in response to climate, soil type and the composition of local biological communities.
2. We tested how soil factors, climate and plant–fungal associations influenced the distribution and concentrations of C and N in MAOM and POM in seven temperate forests in the National Ecological Observatory Network (NEON) across the eastern United States. Samples of upper mineral horizon soil within each forest were collected in plots representing a gradient of dominant tree–mycorrhizal association, allowing us to test how plant and microbial communities influenced POM and MAOM across sites differing in climate and soil conditions.
3. We found that concentrations of C and N in soil organic matter were primarily driven by soil mineralogy, but the relative abundance of MAOM versus POM C was strongly linked to plot-level mycorrhizal dominance. Furthermore, the effect of dominant tree mycorrhizal type on the distribution of N among POM and MAOM fractions was sensitive to local climate: in cooler sites, an increasing proportion of ectomycorrhizal-associated trees was associated with lower proportions of N in MAOM, but in warmer sites, we found the reverse. As an indicator of soil carbon age, we measured radiocarbon in the MAOM fraction but found that within and across sites, $\Delta^{14}C$ was unrelated to mycorrhizal dominance, climate, or soil factors, suggesting that additional site-specific factors may be primary determinants of long-term SOM persistence.
4. *Synthesis*. Our results indicate that while soil mineralogy primarily controls SOM C and N concentrations, the distribution of SOM among density fractions depends on the composition of vegetation and microbial communities, with these effects varying across sites with distinct climates. We also suggest that within biomes, the age of mineral-associated soil carbon is not clearly linked to the factors that control concentrations of MAOM C and N.

KEYWORDS
global change, mineral associated organic matter, mycorrhizal fungi, Plant–soil (below-ground) interactions, soil carbon, soil nitrogen, soil organic matter, temperate forests

1 | INTRODUCTION

Given the vast size of the global carbon (C) pool (Scharlemann et al., 2014), and the desire to promote additional soil C storage, the factors that control the persistence of soil C are of critical concern (Amelung et al., 2020; Bossio et al., 2020; Lal, 2004; Paustian et al., 2019). However, not all components of soil organic matter (SOM) have an equal potential to influence carbon-climate feedbacks, as certain soil pools are often more vulnerable to decay and removal than others (Heckman et al., 2022; Torn et al., 1997). Roughly two-thirds of terrestrial organic C is contained in mineral soils as either particulate organic matter (POM) or mineral-associated organic matter (MAOM; Sokol et al., 2022). Formed from partly decayed plant and faunal biomass, POM is often characterized as vulnerable to continued decomposition, but remains a critical pool of nutrients and carbon in ecosystems where decomposition rates are limited either by climate or the chemical complexity of POM (Haddix et al., 2020; Lugato et al., 2021). In contrast, MAOM is principally composed of small molecular weight organic compounds, derived from either microbial products like exudates and necromass, or from dissolved organic compounds released from plant tissues (Angst et al., 2021). In the process of MAOM formation, these organic molecules become associated with soil mineral surfaces through physical and chemical bonds (Lehmann & Kleber, 2015; Sokol et al., 2018), which may confer some protection against microbial access and further decomposition (Lugato et al., 2021). MAOM is, therefore, a potentially important long-term reservoir of soil C, and there have been many efforts to quantify and characterize MAOM in ecosystems across the globe.

The primary environmental conditions that explain POM and MAOM pool sizes vary widely across study systems (Craig et al., 2022; Haddix et al., 2020; Heckman et al., 2022; Mikutta et al., 2019; Sokol et al., 2022), suggesting that there may be context-specific soil conditions and biological communities that influence their formation and persistence. Suggested drivers of POM and MAOM formation in soil include the quantity and chemistry of organic matter inputs from roots and aboveground litter (Cotrufo et al., 2013; Crow et al., 2009; Keller et al., 2021), microbial community composition and activity (Craig et al., 2018; Frey, 2019; Sollins et al., 2009) and the availability of minerals that effectively bind organic matter, such as poorly crystalline iron oxides (Heckman et al., 2015; Schöning et al., 2005; Torn et al., 1997; Weng et al., 2018). Furthermore, local climate may govern the strength of these drivers across ecosystems (Kramer & Chadwick, 2018). Given this lack of consensus and the wide variation in the spatial influence of these drivers, it is likely that cross-scale interactions (sensu Soranno et al., 2014) between soil mineralogy, microbial communities and organic matter quantity and quality collectively determine MAOM pool sizes, wherein the importance of each factor in controlling SOM dynamics is dependent on the underlying characteristics of the ecosystem. For example, in ecosystems where the availability of poorly crystalline iron oxides is limited or patchy, small-scale variation in soil mineralogy may be the primary determinant of MAOM formation, and organic matter inputs might influence MAOM pool size only where the soil mineral composition is suitable for organic matter sorption (Jones et al., 2015; Kögel-Knabner et al., 2008; Mikutta et al., 2019; Slessarev et al., 2022). In contrast, MAOM formation in ecosystems underlain by soils with high iron oxide content may be primarily influenced by the quantity and quality of organic matter inputs or the activity of plant and microbial communities. This context-dependency is common among drivers of large-scale ecosystem processes (Catford et al., 2022; Hakkenberg et al., 2021; Tedersoo et al., 2016), including SOM dynamics (Hoffland et al., 2020; Kramer & Chadwick, 2018; Rasmussen et al., 2018), reinforcing the need to test these interactions across scales (Nave et al., 2021).

Plant–mycorrhizal associations can also drive within-ecosystem variation in soil C and N cycling and affect the distribution of organic matter as POM and MAOM, particularly in forests. Recent work indicates that in temperate forests where the majority of trees associate with arbuscular mycorrhizal (AM) fungi versus ectomycorrhizal (ECM) fungi, more of the total soil C is stored as MAOM rather than POM (Cotrufo et al., 2019; Craig et al., 2018). This pattern has been attributed to covarying traits of AM- and ECM-associated tree species, such as the typically higher decay rates of AM-associated tree leaf litter (Keller & Phillips, 2019) and to the higher rate of root-derived organic matter inputs in AM-dominated forests (Keller et al., 2021). Therefore, in AM-dominated stands, fast-decomposing litter and large belowground inputs of labile C may stimulate microbial activity and turnover and lead to faster MAOM production than is observed in ECM-dominated stands (Craig et al., 2018). Furthermore, differences in the productivity and activity of mycorrhizal fungi themselves, including hyphal production and turnover and exoenzyme production and organic matter decay, may also influence the formation and stability of POM and MAOM (Frey, 2019). Regardless of the mechanism for MAOM formation in ecosystems with distinct mycorrhizal types, it is unclear whether this pattern—larger proportions of C in MAOM under AM versus ECM trees—is consistent across forest types or dependent on local climate and soil mineralogy.

Despite the generally longer residence time of MAOM compared with POM (Heckman et al., 2022; Swanston et al., 2005), observations of rapid MAOM formation and destabilization under conditions representative of rhizosphere soil suggest that MAOM is composed of some fast-cycling organic matter and some older, more tightly bound organic matter (Fossum et al., 2022; Heckman, Swanston, et al., 2021; Jilling et al., 2021; Keiluweit et al., 2015; Neurath et al., 2021; Swanston et al., 2005). Because MAOM persistence is dictated both by rates of formation and destabilization, concentrations of MAOM C and N in soil do not necessarily reflect MAOM persistence. The potential for MAOM destabilization may be primarily determined by the same factors that influence MAOM formation, including conditions in the soil matrix (Kramer & Chadwick, 2018; Waring et al., 2020) or the particular features of the organo-mineral associations by which MAOM is formed, including both the type and crystallinity of soil minerals as well as the chemical and physical structure of the organic compounds (Heckman et al., 2018;

Kögel-Knabner et al., 2008). Alternatively, MAOM persistence may be driven by a separate suite of ecosystem properties than MAOM formation, including the rate of organic acid production and carbon exudation by roots and microbes (Jilling et al., 2021; Keiluweit et al., 2015), decoupling the rates of formation and destabilization and leading to patterns in MAOM persistence dictated by local conditions.

To assess the strengths of mineralogical, mycorrhizal, and climatic drivers of POM and MAOM C and N content and MAOM C persistence in soils across the eastern United States, we analysed soil collected from plots representing gradients of tree–mycorrhizal associations within seven forested sites in the National Ecological Observatory Network (NEON) that span a range of climate conditions and vary in soil mineralogy. We then compared the relationships between soil oxalate-extractable iron content, mycorrhizal dominance (% basal area of trees associating with either AM or ECM fungi) and climate with several key features of SOM quantity, composition and persistence, including POM and MAOM C and N concentrations, the distribution of soil C and N among POM and MAOM fractions, SOM C:N and MAOM $\delta^{13}C$ and $\Delta^{14}C$. We hypothesized that tree–mycorrhizal associations would influence the concentrations of POM and MAOM C and N and the distribution of C and N among the POM and MAOM fractions but that the effect of dominant tree mycorrhizal type on MAOM and POM would be smaller than the effects of soil mineralogy and climate. Specifically, we predicted that the concentrations of MAOM C and N would be higher in sites with high soil iron oxide content and in warmer climates, where conditions favour rapid organic matter incorporation into soil, and mineral surfaces suitable for sorption are abundant. Based on recent work from temperate forests, we also predicted that AM-dominated stands would generally have higher proportions of SOM C and N in the MAOM fraction relative to ECM-dominated stands (Cotrufo et al., 2019; Craig et al., 2018). Furthermore, we expected that the same factors that lead to higher concentrations of MAOM C and N would generally correspond with longer MAOM residence times (estimated using MAOM $\Delta^{14}C$) and a higher degree of microbial processing, indicated by higher $\delta^{13}C$ and lower MAOM C:N.

2 | MATERIALS AND METHODS

2.1 | Soil sampling

We obtained mineral horizon soil samples from study plots located within seven forests in the National Ecological Observatory Network (Figure 1) from the NEON Biorepository at Arizona State University (https://biorepo.neonscience.org/portal/). Soil samples were collected during the growing season between 2014 and 2020 following standard NEON protocols (Hinckley et al., 2016). Samples were collected from the upper 30 cm of the soil profile, unless rocks or other site characteristics prevented coring to this depth; in such cases, the maximum accessible depth was used. Within each plot, cores were collected in a number sufficient to provide the necessary soil mass for chemical and physical analyses. Organic and mineral horizon soils were separated, and in cases where multiple cores were collected within a plot, samples were aggregated and homogenized by horizon to represent the soil conditions at the plot scale. Samples were air-dried and sieved to 2 mm prior to archiving. Forest sites were chosen for this study based on the availability of physical soil samples suitable for representing within-site variation in tree mycorrhizal type (for site descriptions, see Table 1). Plots within each site (TREE: $n = 6$, all others: $n = 7$) were selected to represent the largest possible range of dominance by AM- versus ECM-associated tree species at the plot level within each site (Figure 1b).

2.2 | Data selection and processing

The mycorrhizal dominance (i.e. %ECM and %AM tree basal area) of each study plot was calculated using tree basal area and species identity data from the Vegetation Structure data set on the NEON Data Portal: https://data.neonscience.org/data-products/DP1.10098.001 (NEON, 2022b). To assess tree species composition, we used woody vegetation data for the most recent year of sampling at the time of data download from each study site, excluding years where sampling efforts were interrupted by external factors or where data collection was otherwise incomplete. We filtered

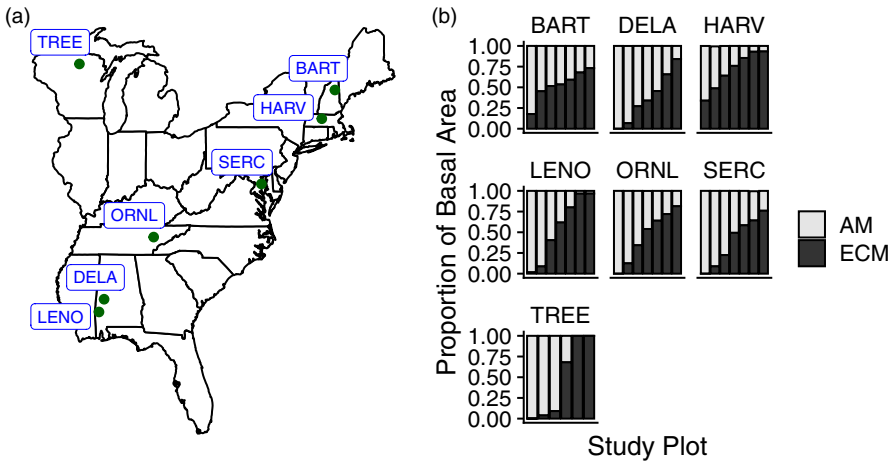

FIGURE 1 (a) Locations of seven NEON temperate forest sites used in this study (b) Proportion of basal area attributed to arbuscular mycorrhizal (AM)- and ectomycorrhizal (ECM)-associated tree species within the plots where soil was collected in each site.

TABLE 1 Location of study sites with mean climate conditions, soil order and dominant AM and ECM tree species in the selected study plots by basal area. Climate decomposition index (CDI) was determined using the Lloyd and Taylor (1994) calculations described in Adair et al. (2008).

Site	Location	MAT (°C)	MAP (mm)	Dominant soil order	Climate decomposition index	Dominant AM tree species	Dominant ECM tree species
Treehaven (TREE)	Lincoln County, WI 45.49369°N −89.58571°W	4.8	797	Spodosol	0.2151	*Acer rubrum* *Acer saccharum*	*Pinus strobus* *Picea mariana*
Bartlett Experimental Forest (BART)	Carroll County, NH 44.063889°N −71.287375°W	6.2	1325	Spodosol	0.5097	*Acer rubrum* *Fraxinus americana*	*Fagus grandifolia Tsuga canadensis*
Harvard Forest (HARV)	Worcester County, MA 42.53691°N −72.17265°W	7.4	1199	Inceptisol	0.5823	*Acer rubrum* *Fraxinus americana*	*Tsuga canadensis* *Quercus rubra*
Smithsonian Environmental Research Center (SERC)	Anne Arundel County, MD 38.890131°N −76.560014°W	13.6	1075	Ultisol	0.7565	*Liriodendron tulipifera* *Liquidambar styraciflua*	*Quercus alba* *Fagus grandifolia*
Oak Ridge National Lab (ORNL)	Anderson County, TN 35.964128°N −84.282588°W	14.4	1340	Ultisol	0.9641	*Liriodendron tulipifera* *Acer rubrum*	*Quercus alba* *Quercus montana*
Dead Lake (DELA)	Greene County, AL 32.541727°N −87.803877°W	17.6	1372	Ultisol	1.1919	*Acer rubrum* *Celtis laevigata*	*Pinus taeda* *Quercus michauxii*
Lenoir Landing (LENO)	Choctaw County, AL 31.853861°N −88.161181°W	18.1	1386	Inceptisol	1.2360	*Liquidambar styraciflua* *Platanus occidentalis*	*Quercus pagoda* *Quercus laurifolia*

these data to include only live individuals with measurements of stem diameter and with either a species or genus-level identification. Woody vines were excluded from the dataset. Mycorrhizal association of each species was determined using the USDA PLANTS database (USDA, NRCS. National Plant Data Team., 2021), and plot-level AM and ECM dominance was calculated by dividing the total basal area of all AM-associated trees and all ECM-associated trees from the total basal area in each plot. Where tree species were not known, we used genus to assign dominant mycorrhizal type to individual stems. Trees associated with ericoid mycorrhizal fungi were present in eight of the study plots and constituted no more than ~0.5% of the basal area in any one plot (Table S1). To assess associations between tree mycorrhizal type and leaf litter production, we used data from the Litterfall and fine woody debris production and chemistry data set from the NEON data portal: https://data.neonscience.org/data-products/DP1.10033.001 (NEON, 2022a). These data were filtered to include only leaf and needle litter, and only data collected in the most recent years when sampling was not disrupted by external factors to maximize the available dataset. These years ranged from 2016 to 2019. The mean annual litterfall mass for each study plot was calculated as the mean value of the annual sum of all leaf and needle litter mass from each study plot. NEON datasets were accessed and merged using the neonUtilities package in R (Lunch et al., 2021).

2.3 | Soil chemical analyses

We separated air-dried mineral soil samples into particulate and mineral-associated forms of organic matter with density fractionation (Sollins et al., 2009) using sodium polytungstate (SPT) adjusted to a density of 1.7 g/mL. Briefly, approximately 5 g of mineral horizon sample was submerged in SPT solution and centrifuged to isolate loose, floating organic material (hereafter the free particulate organic matter [fPOM] fraction). Then, particulate matter contained within soil aggregates was separated from the remaining material by shaking the sample to disrupt aggregates for 18 h at 200 oscillations per minute and centrifugation to isolate material with a density less than 1.7 g/mL (hereafter the occluded particulate organic matter [oPOM] fraction). The remaining organic matter was considered mineral-MAOM. Following separation, all organic matter fractions were rinsed of residual SPT using Nanopure water, oven dried and analysed for percent carbon and nitrogen using an elemental combustion system (Costech Analytical Technologies). The SPT solution was standardized to a density of 1.7 g/mL for all samples, which was deemed sufficient for clear separation of SOM pools with centrifugation following visual inspection.

Isolated MAOM from mycorrhizal gradient plots in six of the NEON sites was analysed for $\delta^{13}C$ and $\Delta^{14}C$. Samples were analysed for $\delta^{13}C$ at the Stable Isotope Research Facility in the Department of Earth and Atmospheric Sciences at Indiana University. Samples were run on an elemental combustion system (Costech ECS 4010; Costech Analytical Technologies) attached to an isotope ratio mass spectrometer (Thermo Finnigan DELTA Plus XP IRMS) with a gas bench interface. $\Delta^{14}C$ measurements were conducted at the Center for Accelerator Mass Spectrometry at Lawrence Livermore National Laboratory (as per McFarlane et al., 2013). Samples were not pretreated to remove carbonates due to the relatively acidic conditions observed in soils from these sites; mean soil pH in each site ranged from 4.33 (BART) to 5.54 (DELA). Samples from ORNL were not included in isotope analyses due to ^{14}C contamination from a nearby hazardous waste incinerator (Trumbore et al., 2002). Samples were combusted and converted to graphite (Vogel et al., 1984) and analysed on the NEC 1.0 MV Tandem Accelerator Mass Spectrometer (Broek et al., 2021). The ^{14}C content of each sample was reported in $\Delta^{14}C$ notation, corrected for mass-dependent fractionation with measured $\delta^{13}C$ values and then corrected to the year of measurement (2021) for ^{14}C decay since 1950 (Stuiver & Polach, 1977).

To determine oxalate-extractable iron content, a 0.2 g subsample of bulk mineral soil from each study plot was submerged in 20 mL of a 0.2 M oxalate extracting solution, shaken at low speed for 4 h in the dark, centrifuged for 15 min at 2500 rpm and filtered through grade 1 qualitative filter paper (Whatman). Extracts were then analysed for iron content on a mass percent basis with atomic absorption spectrometry (PerkinElmer Instruments).

2.4 | Climate decomposition index

We extracted monthly temperature and precipitation data for each NEON site for the year 2017 using the Parameter-elevation Regressions on Independent Slopes Model (PRISM) dataset (PRISM Climate Group, Oregon State University, n.d.). We then calculated the climate decomposition index (CDI) of each site to represent the overall climate using the temperature functions described by Lloyd and Taylor (1994) following Adair et al. (2008). The CDI of each site is a function of minimum and maximum monthly temperature and monthly precipitation and represents an integrated index of conditions important for influencing decomposition. Higher CDI values indicate warmer or wetter sites; for the seven forests studied here, mean annual precipitation was less variable than mean annual temperature, so CDI values primarily reflect differences in site temperature (Table 1).

2.5 | Statistical analysis

To address our hypothesis that climate, soil mineralogy and mycorrhizal dominance influence SOM interactively, we constructed a suite of linear models for the proportions of total soil C and N stored in each density fraction as well as the concentrations of MAOM and POM C and N per gram of mineral soil. These models include plot-level mycorrhizal dominance and soil FeOx content and site-level CDI as fixed effects, with study site as a random intercept (Bates et al., 2015). Because we expected the effects of these variables to change across climate and soil conditions, we also tested all pairwise

interactions between our fixed effects but included interaction terms in the final models only when they significantly influenced SOM fractions. Finally, we compared models of MAOM C and N content using each site's mean annual temperature in place of CDI; both methods yielded the same patterns, so we present models using CDI to represent variability in both temperature and precipitation across sites. One sample from Harvard Forest (HARV) with an exceedingly high value of fPOM C and N concentration (>20 standard deviations above mean fPOM C concentration; >6 standard deviations above mean fPOM N concentration) was removed from these analyses for a total of 47 observations. Additionally, we constructed linear models with the same fixed and random effects to test how the C:N of each density fraction, as well as the $\delta^{13}C$ and $\Delta^{14}C$ of the MAOM fraction, responded to mycorrhizal associations, FeOx content and climate. We also used a series of simple linear models to assess whether the MAOM C concentrations or the proportions of C in the MAOM fraction were associated with MAOM C isotope ratios. Linear mixed effects models were constructed with the LME4 package in R (v. 4.0.2; Bates et al., 2015).

To further investigate how patterns in leaf litter production may have influenced our results, we constructed simple linear models of leaf litter mass across AM-ECM tree gradients within each NEON study site. For this analysis, we gathered data from all plots for which appropriate litter mass data were available from the NEON data portal; therefore, these plots do not necessarily correspond to those from which we were able to acquire soil samples for density fractionation, instead representing the general patterns in litter production with respect to tree mycorrhizal associations within each site.

3 | RESULTS

3.1 | Distribution of soil C and N among density fractions

To test our hypothesis that tree–mycorrhizal associations influence the formation of POM and MAOM, we assessed how the proportion of C and N in MAOM versus POM varied with the dominant mycorrhizal type of the trees in our study plots. The mean percentage of total soil C [80 ± 1.1%] and N [89 ± 0.9%] contained in the MAOM fraction was fairly consistent across study sites, but within sites, the MAOM C and N proportion generally decreased along gradients of AM to ECM tree dominance in the forest plots (Table 2). With increasing ECM-associated tree basal area, we found that the proportion of C in particulate fractions (both fPOM and oPOM) increased (fPOM: $t_{41} = 2.27$, $p = 0.029$; oPOM: $t_{41} = 2.28$, $p = 0.028$), and in turn, the proportion of C in MAOM decreased ($t_{41} = -3.30$, $p = 0.002$) within the majority (6 out of 7) of our study sites (Figure 2). In one site (LENO), we observed the opposite pattern, where a higher proportion of C in the MAOM was associated with greater ECM tree

TABLE 2 Effects of mycorrhizal dominance (% ECM basal area), climate decomposition index (CDI), soil oxalate-extractable iron content (FeOx) and the interaction between mycorrhizal dominance and CDI on the proportions of total soil C and N in each SOM fraction, and the concentrations of fPOM, oPOM and MAOM C and N in mineral soil (mg C within each fraction per gram of bulk soil) from plots located within seven forests in the National Ecological Observatory Network (NEON). Interactions terms were only included in final models when they were found to significantly influence SOM fractions. Standardized estimates are presented to allow comparison of the strengths of different drivers within models. Standardized standard errors follow in parentheses. Statistical significance indicates with asterisks: $^{*}p < 0.10$; $^{**}p < 0.05$; $^{***}p < 0.001$. For mycorrhizal dominance, a negative estimate reflects lower values of the response variable with increasing ECM tree dominance. Site included as a random intercept; for random-effect variance see Table S2.

SOM fraction	Predictor	Proportion of C Std β (Std SE)	Concentration of C Std β (Std SE)	Proportion of N Std β (Std SE)	Concentration of N Std β (Std SE)
fPOM	(Intercept)	−0.00 (0.14)***	−0.01 (0.25)**	0.00 (0.14)***	−0.01 (0.24)**
	% ECM	0.29 (0.13)**	0.17 (0.12)	0.22 (0.13)	0.10 (0.12)
	CDI	−0.12 (0.15)	−0.39 (0.26)	−0.35 (0.16)**	−0.40 (0.26)
	FeOx	−0.51 (0.15)**	−0.08 (0.17)	−0.30 (0.15)*	−0.04 (0.17)
	% ECM × CDI	*na*	*na*	*na*	*na*
oPOM	(Intercept)	0.00 (0.18)**	0.00 (0.21)**	−0.02 (0.14)	0.01 (0.22)**
	% ECM	0.33 (0.15)**	0.21 (0.13)	0.17 (0.14)	0.09 (0.13)
	CDI	0.10 (0.20)	−0.38 (0.23)	−0.38 (0.16)**	−0.40 (0.24)
	FeOx	−0.17 (0.18)	0.23 (0.18)	0.05 (0.16)	0.27 (0.18)
	% ECM × CDI	*na*	*na*	−0.25 (0.12)**	*na*
MAOM	(Intercept)	0.00 (0.15)***	0.00 (0.29)**	0.02 (0.12)	0.01 (0.20)
	% ECM	−0.42 (0.13)**	−0.07 (0.11)	−0.23 (0.12)*	−0.05 (0.11)
	CDI	0.03 (0.17)	−0.58 (0.29)*	0.46 (0.14)**	−0.20 (0.21)
	FeOx	0.50 (0.16)**	0.60 (0.15)***	0.15 (0.14)	0.78 (0.15)***
	% ECM × CDI	*na*	*na*	0.20 (0.11)*	0.18 (0.09)*

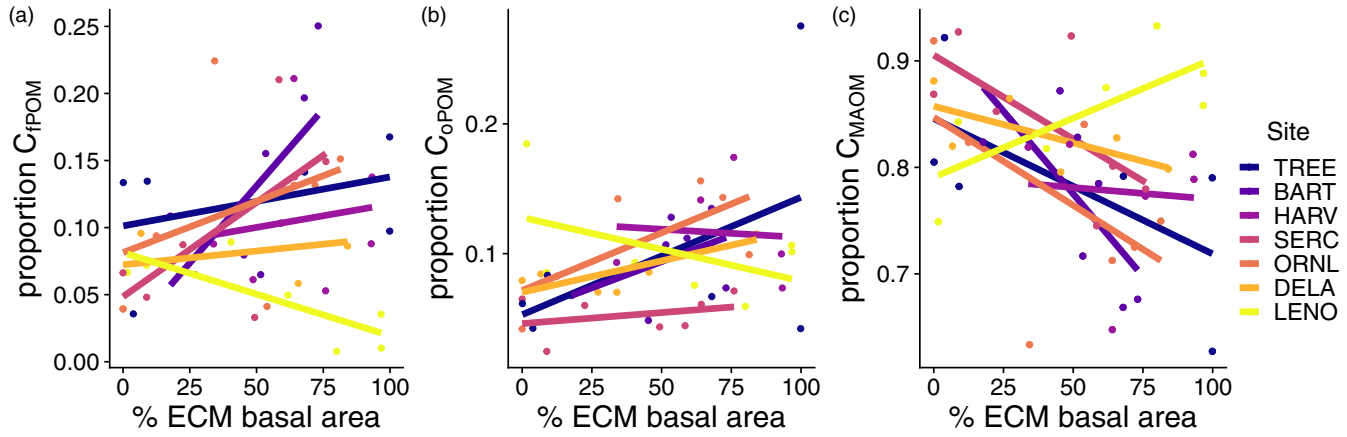

FIGURE 2 Proportions of total soil C in the (a) free particulate fraction (C_{fPOM}), (b) occluded particulate fraction (C_{oPOM} and (c) mineral-associated organic matter (C_{MAOM}) fraction in plots situated along a gradient of tree mycorrhizal dominance in seven forested NEON sites (see Table 1 for site definitions). Points represent individual plots within each study site ($n = 46$). Lines reflect the best fit from linear models specific to each study site.

dominance ($F_{1,5} = 6.554$, $p = 0.0506$). However, combining all sites, the mean percentage of total soil C in the MAOM fraction decreased by 8.0% across a gradient of 100% AM to 100% ECM tree basal area.

The proportion of soil N in the MAOM fraction (Figure S1) tended to respond differently to mycorrhizal dominance under different climate conditions ($t_{40} = 1.94$, $p = 0.063$; Table 2); in cooler sites, the proportion of soil N in the MAOM fraction declined with increasing dominance of ECM-associated tree species, but increased with ECM dominance in warmer sites (Figure 3). The proportion of N in the oPOM fraction showed the reverse, with stronger positive relationships with ECM dominance in colder sites ($t_{40} = -2.09$, $p = 0.043$; Table 2). To better assess how differences in organic matter inputs may have influenced the patterns we observed along AM to ECM-dominated gradients, we compared leaf and needle litter production with tree mycorrhizal type in all seven forests; the dry mass of leaf and needle litter was negatively associated with plot-level ECM tree dominance in only two sites: TREE ($F_{1,18} = 22.65$; $p < 0.001$) and BART ($F_{1,18} = 8.95$; $p = 0.008$; Figure S2).

3.2 | Mineralogical and climatic controls on SOM C and N

Because soil mineralogy and climate-driven weathering are recognized as key determinants of mineral-organic matter relationships (Rasmussen et al., 2018; Slessarev et al., 2022), we tested how bulk soil oxalate-extractable iron (FeOx) concentration and site-level CDI influenced the concentrations of MAOM and POM C and N. Bulk soil FeOx concentration was strongly associated with higher concentrations of MAOM C ($t_{41} = 3.97$, $p < 0.001$) and N ($t_{41} = 4.87$, $p < 0.001$; Figure 4) but was not an important predictor of oPOM or fPOM concentrations (Table 2). MAOM C concentrations were marginally negatively associated with CDI; in other words, warmer sites tended to have overall lower MAOM C concentrations (Table 2). For MAOM N concentrations, however, we found a similar trend to that of MAOM N proportions: climate influenced the effect of mycorrhizal type on the concentration of MAOM N in the soil, wherein warmer sites showed increases in MAOM N concentrations with increasing ECM dominance ($t_{40} = 1.95$, $p = 0.058$; Table 2). Furthermore, FeOx concentration was also positively associated with the proportion of C in MAOM ($t_{41} = 3.17$, $p = 0.003$), but not with the proportion of N in MAOM (Table 2).

3.3 | Patterns in soil organic matter C:N and mineral-associated organic matter carbon isotopes

To better understand the pathways of MAOM formation, turnover and SOM origin, we assessed how mineralogical, climatic and microbial drivers impacted SOM fraction C:N and the isotopic composition of MAOM C. The C:N of all three density fractions generally increased with ECM dominance, but this effect was strongest in the POM fractions (Figure 5; Table 3). In addition, MAOM C:N was significantly lower in warmer sites ($t_{41} = -3.24$, $p = 0.002$), while neither the fPOM nor oPOM C:N was associated with site climate (Table 3). Finally, the fPOM C:N was negatively associated with FeOx concentration ($t_{41} = -2.67$, $p = 0.011$; Table 3).

We measured the radiocarbon content of the MAOM fraction as an estimate of the carbon age to illuminate possible drivers of MAOM persistence. The $\Delta^{14}C$ of the soil MAOM fraction varied substantially across six of the forest sites (ORNL omitted from this analysis due to environmental ^{14}C contamination; Figure 6) but was not correlated with any of the soil, climate, or plant-fungal variables that we tested (Table 4; Figure S3), nor was it related to the MAOM C concentrations ($F_{1,39} = 0.215$; $p = 0.65$) or proportions of C in MAOM ($F_{1,39} = 0.044$; $p = 0.83$). MAOM in most sites was near modern in origin, with the least modern C in the MAOM fraction at Dead Lake, AL (DELA) and the most modern C incorporated into MAOM at the Smithsonian Environmental Research Center (SERC).

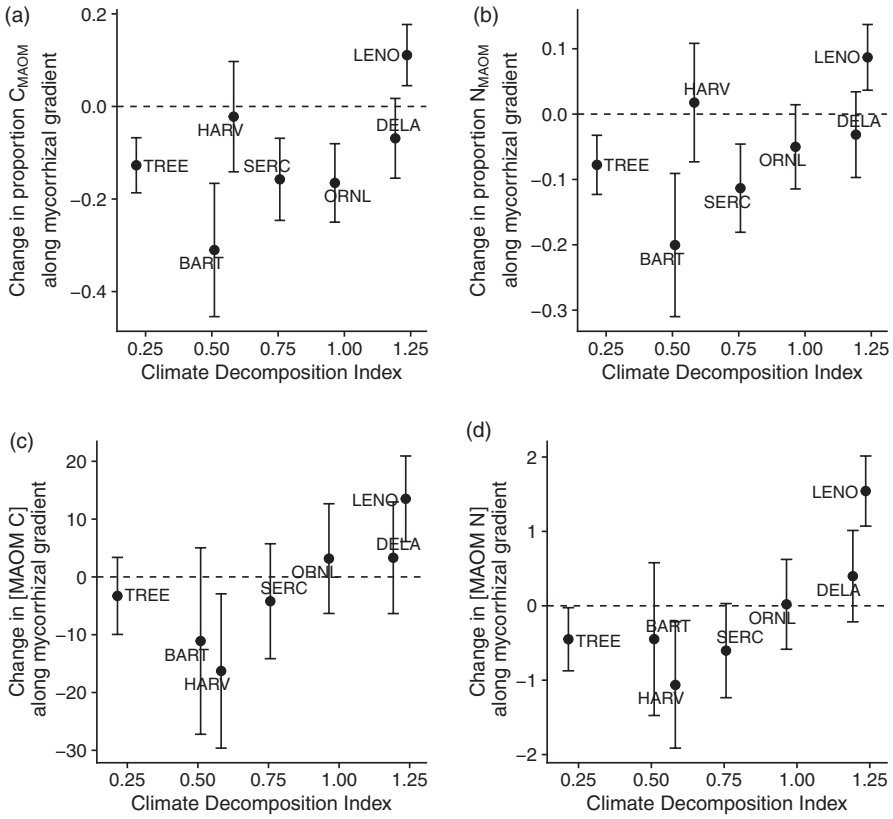

FIGURE 3 The influence of tree mycorrhizal dominance (% ECM tree basal area) on MAOM C (a, c) and N (b, d) proportions and concentrations in seven forested NEON sites with respect to climate decomposition index (CDI). CDI represents the mean values and variability of monthly temperature and precipitation in each site (see Section 2 for details). Each point represents the slope of the relationship between MAOM C or N and plot-level ECM dominance within a site (as in Figure 2). Bars indicate standard error of the slopes. Panels a and b show the strength and direction of changes in the proportion of C and N in MAOM with increasing ECM tree dominance in each site, while panels c and d show the strength and direction of changes in the concentrations of mineral-bound C and N with increasing ECM dominance. Points above the dotted line represent positive slopes (i.e. soils in these sites have a positive association between MAOM C or N and ECM dominance; $n = 7$ for all sites except TREE and HARV [$n = 6$]).

FIGURE 4 Concentrations of MAOM C and N in soils from 7 forested NEON sites (see Table 1 for site abbreviations) versus concentrations of oxalate-extractable iron (FeOx) in bulk surface mineral soils. Individual points represent measured values of FeOx from the same bulk mineral soil samples used to determine MAOM and POM content via density fractionation ($n = 46$).

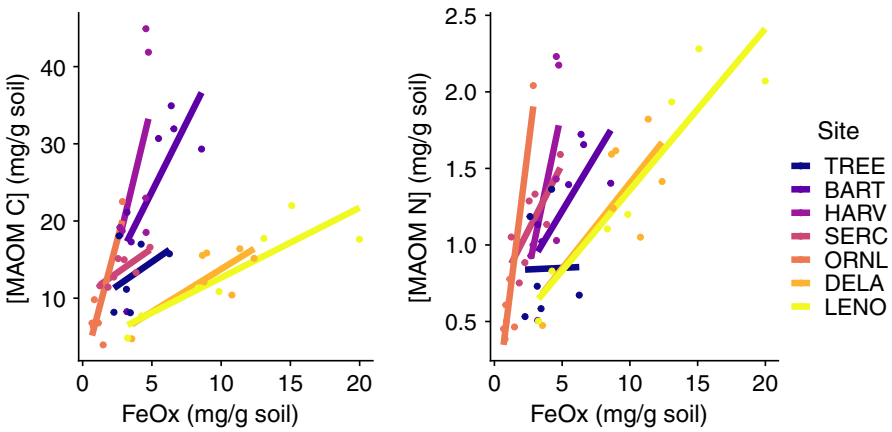

MAOM $\delta^{13}C$ signatures were positively associated with soil FeOx content, although this relationship was driven primarily by samples from Lenoir Landing, AL (LENO), which had the highest values of oxalate-extractable iron content of any site (Table 4). We also observed a negative association between CDI and MAOM $\delta^{13}C$, but the size of this effect was minimal (−0.03‰ across the range of CDI values represented by our sites; Figure S3). Finally, MAOM $\delta^{13}C$ signatures were not associated with either MAOM C concentrations ($F_{1,39} = 0.004$; $p = 0.94$) or the proportion of C in the MAOM fraction ($F_{1,39} = 0.47$; $p = 0.50$).

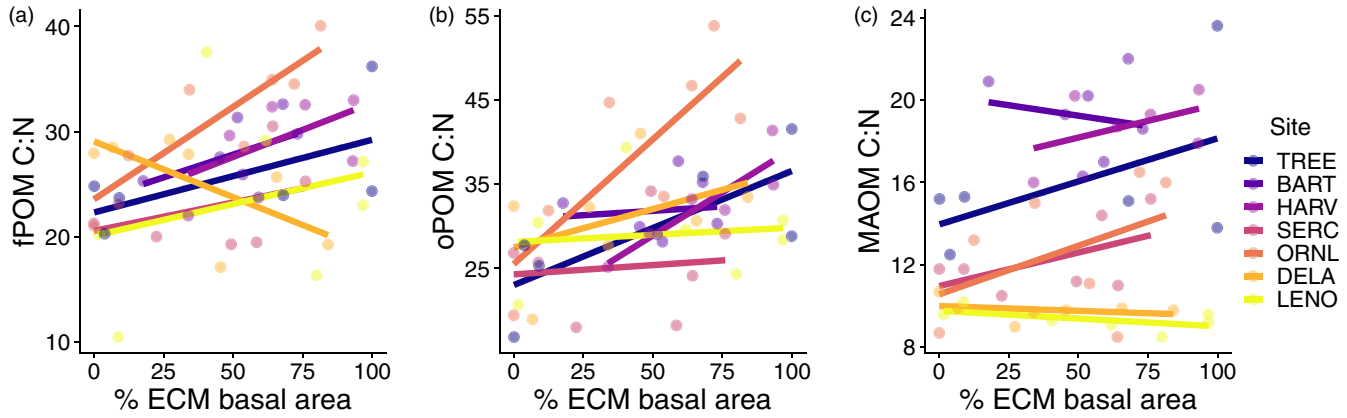

FIGURE 5 SOM C:N in soils from 7 forested NEON sites (see Table 1 for site abbreviations) along gradients of tree–mycorrhizal associations ranging from AM-dominated to ECM-dominated forest plots within each site. Individual points represent measured ratios of carbon to nitrogen in density-fractionated fPOM, oPOM and MAOM samples ($n = 47$).

TABLE 3 Effects of mycorrhizal dominance (% ECM basal area), climate decomposition index (CDI), and soil oxalate-extractable iron content (FeOx) on the ratio of carbon to nitrogen in each SOM density fraction from plots located within seven forests in the National Ecological Observatory Network (NEON). Standardized estimates are presented to allow comparison of the strengths of different drivers within models. Standardized standard errors follow in parentheses. Statistical significance indicates with asterisks: *$p < 0.10$; **$p < 0.05$; ***$p < 0.001$. For mycorrhizal dominance, a positive estimate reflects higher C:N with increasing ECM tree dominance. Site included as a random intercept; for random-effect variance, see Table S3.

		C:N
SOM fraction	Predictor	Std β (Std SE)
fPOM	(Intercept)	0.00 (0.17)***
	% ECM	0.41 (0.13)**
	CDI	0.13 (0.19)
	FeOx	−0.44 (0.17)**
oPOM	(Intercept)	0.00 (0.20)***
	% ECM	0.49 (0.13)***
	CDI	0.19 (0.22)
	FeOx	−0.22 (0.17)
MAOM	(Intercept)	0.00 (0.21)***
	% ECM	0.17 (0.08)**
	CDI	−0.69 (0.21)**
	FeOx	−0.03 (0.12)

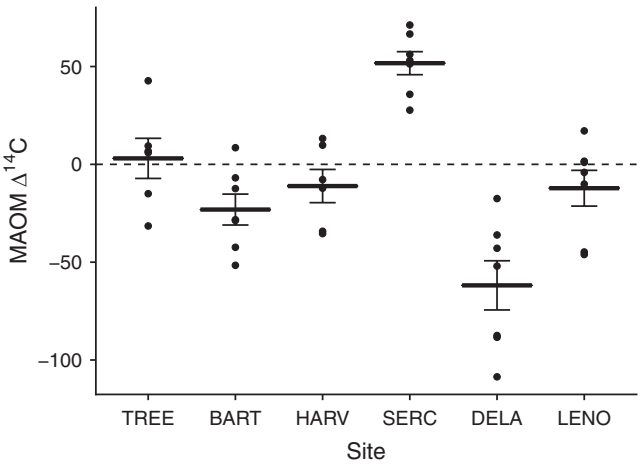

FIGURE 6 Mean (±SE) $\Delta^{14}C$ of MAOM from six NEON temperate forests (ORNL was omitted due to site-level ^{14}C contamination). Values greater than zero indicate a modern origin of MAOM C with shorter turnover times; negative values indicate older C (i.e. C fixed pre-1950). Individual points represent MAOM isolated from mineral horizon soil samples (0–30 cm) collected along tree-mycorrhizal gradients within each site. Sites ordered by increasing climate decomposition index.

4 | DISCUSSION

4.1 | Tree mycorrhizal associations influence the relative abundance of mineral-associated organic matter and POM C within sites

We show that the dominance of AM- versus ECM-associated tree species is associated with the relative abundance of MAOM C and POM C within eastern temperate forests; beneath AM trees, a higher proportion of soil carbon was found in the MAOM fraction compared to the POM fraction, while the reverse was true beneath ECM trees. Notably, this pattern was consistent in all but one site (Figure 2), and the additional variance in MAOM and POM C proportions explained by other features of each site not measured in this study (i.e. the random effect of site) was small or negligible (Table S2). These results add to the body of evidence that mycorrhizal communities present in soil may influence the likelihood that incoming organic matter becomes mineral-bound (Cotrufo et al., 2019; Craig et al., 2018). Differences between forests dominated by tree species with AM versus ECM associations, in particular, may arise from variation in decomposition processes beneath AM- and ECM-associated trees. Previous studies show that both

TABLE 4 Effects of mycorrhizal dominance (% ECM basal area), climate decomposition index (CDI) and soil oxalate-extractable iron content (FeOx) on MAOM $\delta^{13}C$ and $\Delta^{14}C$ from plots located within seven forests in the National Ecological Observatory Network (NEON). Standardized estimates are presented to allow comparison of the strengths of different drivers within models. Standardized standard errors follow in parentheses. Statistical significance indicated with asterisks: $^{*}p<0.10$; $^{**}p<0.05$; $^{***}p<0.001$. For mycorrhizal dominance, a positive estimate reflects higher C:N with increasing ECM tree dominance. Site included as a random intercept; for random effect variance see Table S4.

	$\delta^{13}C$	$\Delta^{14}C$
Predictor	**Std β (Std SE)**	**Std β (Std SE)**
(Intercept)	−0.01 (0.14)***	−0.01 (0.40)
% ECM	−0.02 (0.15)	−0.09 (0.10)
CDI	−0.49 (0.18)**	−0.42 (0.42)
FeOx	0.65 (0.19)**	0.18 (0.14)

microbial community composition and activity can vary with tree mycorrhizal type (Carteron et al., 2020; Cheeke et al., 2016; Fitch et al., 2020; Moore et al., 2015; Singavarapu et al., 2022), but the extent to which these changes influence MAOM formation is difficult to test. Mycorrhizal association type is often strongly associated with related factors that are likely to impact SOM decay and sorption, including the quality of organic matter inputs (Cornelissen et al., 2001; Huang et al., 2022; Keller & Phillips, 2019), the composition of the free-living bacterial and fungal communities (Carteron et al., 2020; Fitch et al., 2020; Singavarapu et al., 2022) and the production of organic compounds by roots and mycorrhizal fungi themselves (Keller et al., 2021). Indeed, the generally higher C:N of POM beneath ECM trees in most sites (Figure 5) suggests that lower quality plant litters in these plots may have led to relatively slower decomposition rates than beneath AM trees, contributing to the lower proportion of C in MAOM versus POM in ECM-dominated plots.

4.2 | Climate mediates the effect of mycorrhizal fungi on soil organic matter nitrogen

The effect of tree-mycorrhizal dominance on both the concentration of MAOM N and the abundance of MAOM N versus POM N varied across sites, implying that the role of mycorrhizal fungi in soil nitrogen dynamics may be context-dependent. Specifically, we noted a trend suggesting that in cooler sites, more soil N may be found in the MAOM fraction beneath AM-associated trees but that in warmer sites, more of the total soil N may be found in the MAOM fraction in ECM-dominated forests. Although these trends were not as strong as those showing greater proportions of MAOM C beneath AM trees, they suggest that the mechanisms by which microbes influence SOM C distributions do not equally influence SOM N distributions and that these mechanisms potentially vary along biophysical gradients such as climate.

A possible explanation for the variable MAOM N response to mycorrhizal type across sites may be that the primary origin of the mineral-bound organic matter may differ with site climate (Angst et al., 2021; Liang et al., 2019). Molecular analyses of MAOM from other NEON sites show that MAOM in forests receiving >1200 mm precipitation annually with ratios of MAOM C to N greater than 15 may be primarily composed of plant-derived, rather than microbially derived organic matter (Yu et al., 2022). In our study, these conditions are found at BART and HARV (Figure 5; Table 1), and an MAOM C:N greater than 15 was also commonly observed at TREE. These three sites represent the coldest sites, and in both TREE and BART, we also noted that leaf litter inputs are lower in ECM-dominated plots versus AM-dominated plots (Figure S2). Therefore, the decline in MAOM N concentration with ECM dominance in these sites may be partly explained by a smaller contribution of plant-derived dissolved organic matter, owing to the generally slower decomposition rate of ECM leaf litter in cooler temperate forests (Keller & Phillips, 2019), smaller inputs of aboveground litter in ECM-dominated plots (Figure S2), or lower rates of root-derived organic matter input from ECM versus AM trees (Keller et al., 2021). This explanation is broadly supported by other studies showing larger MAOM N pools beneath AM versus ECM vegetation in other temperate forests (Cotrufo et al., 2019; Craig et al., 2018).

The positive relationships we found between the proportions and concentrations of MAOM N and ECM tree dominance in the warmer sites are not as widely supported by existing literature. These relationships are particularly strong at LENO and DELA, both located in central Alabama, USA; however, the potential mechanisms behind the patterns may be distinct at these two sites. At LENO, ECM tree dominance is positively correlated with soil FeOx content, so higher concentrations of MAOM N beneath ECM trees in this site are likely due to corresponding differences in soil mineral suitability (Keiluweit et al., 2012; Swenson et al., 2015). At DELA, it is possible that tree species exhibit preferences for other soil conditions that also correspond to tree mycorrhizal type; for example, ECM-associated trees may be abundant in wetter microsites, where decomposition is limited by seasonal inundation and water-filled pore space allows for the rapid transport of low-molecular-weight organic compounds to mineral surfaces (Waring et al., 2020). However, MAOM in these sites also had the lowest C:N ratios, indicating a greater influence of microbially derived organic matter in the mineral soil (Figure 5), and it has been suggested that the proportion of microbial contributions to MAOM predominate with increasing mean annual temperature (Angst et al., 2021). Therefore, we suggest that in these warmer sites, fungal tissues may constitute a larger proportion of the organic inputs forming MAOM. Given that ECM-associated trees are thought to invest more in mycorrhizal tissue production than in root tissue production compared to AM-associated trees (Jevon & Lang, 2022; Tedersoo & Bahram, 2019), it is possible that in warmer forests, soil beneath ECM-dominated stands stores more N in the MAOM fraction, in part, due to the turnover of chitin-rich ECM fungal hyphae (Fernandez et al., 2016). If so, the primacy of fungal versus plant-derived tissues as precursors to MAOM may also account for the

fact that the interaction we noted between the role of mycorrhizal type and climate for MAOM N proportions and concentrations was not detected for MAOM C proportions and concentrations (Table 2).

In addition to factors that influence the rate of MAOM N accumulation, destabilization and removal of N from soil mineral surfaces may also contribute to patterns in MAOM N concentrations with tree mycorrhizal type and decouple MAOM C from MAOM N dynamics. These mechanisms may be particularly important in cooler sites, where decomposition rates are lower and N limitation of primary productivity is potentially greater than in warmer sites, leading to N mining by plant roots and mycorrhizae from mineral-bound organic matter (Jilling et al., 2018; Lambers et al., 2008; Lovett et al., 2018). Given that some species of ECM fungi have retained the ability to depolymerize organic matter as a source of N for their plant hosts (Pellitier & Zak, 2018), it is possible that N mining by ECM fungi may contribute to lower concentrations of MAOM N beneath ECM trees in cooler sites. Both of these processes—higher MAOM N inputs from AM-associated tree litter and potential removal by ECM fungal mining—may weaken in strength in warmer climates, where differences in leaf litter decay rates between AM and ECM trees are generally smaller (Keller & Phillips, 2019), and where higher POM decomposition rates may reduce the need for N mining from mineral soil as a dominant pathway of plant N uptake.

4.3 | Effects of soil mineralogy and climate on mineral-associated organic matter C and N

Across our study sites, we found that the concentrations of MAOM C and N in soil were primarily explained by soil mineralogy. The concentration of oxalate-extractable iron in soil (FeOx), representing the abundance of the poorly crystalline mineral phases best suited for forming organo-mineral associations (Kleber et al., 2005), was the factor most strongly and positively associated with MAOM C and N concentrations among those we tested. On average, a 1% increase in soil FeOx concentration led to an increase of 32 mg of MAOM C and 2.4 mg of MAOM N per gram of soil. This pattern has been observed previously, strengthening the evidence that mineralogy controls MAOM content despite the large variation in soil order, climate and forest species composition among our sites (Heckman et al., 2015; Kögel-Knabner et al., 2008; Mikutta et al., 2006; Slessarev et al., 2022; Torn et al., 1997; Weng et al., 2018). Furthermore, climate influenced the concentration of MAOM C. We expected that warmer or wetter conditions would accelerate litter leaching and POM decomposition, leading to faster production of the small-molecular weight compounds that form the bulk of MAOM and resulting in higher MAOM C and N concentrations and lower POM C and N concentrations. Instead, we found that warmer sites generally had lower concentrations of MAOM C and that climate did not significantly influence the concentrations of POM C or N (Table 2). These patterns are surprising given theorized differences in the temperature sensitivity of POM and MAOM decomposition: POM decomposition is generally considered to be more sensitive to temperature than MAOM decomposition, given that (a) rates of microbial activity influencing POM decay are highly dependent on temperature and (b) the strength of the physical bonds between organic matter and minerals in MAOM are not necessarily dependent on temperature (Lugato et al., 2021). However, there is ample evidence for MAOM destabilization in the soil rhizosphere, indicating that root and microbial activity can, in certain conditions, lead to MAOM decomposition and C loss as microbial respiration. This outcome may be more likely in warmer sites, where high rates of root and microbial activity may lead to microbes using MAOM C as an energy source. Thus, any MAOM C gained by higher rates of POM decay and greater organic matter export to soil mineral surfaces may be offset by C losses from MAOM decomposition. This explanation is further supported by the lower MAOM C:N in warmer sites (Table 3).

Across large spatial scales, the effects of climate on MAOM C may also be modified by corresponding changes in (1) soil weathering rate and, subsequently, the availability of poorly crystalline mineral phases (Slessarev et al., 2022) or (2) primary productivity, which controls the rate of organic matter inputs to soil. While we found that plot productivity, represented by tree basal area, was not related to the CDI of our study sites ($F_{1,46} = 0.056$; $p = 0.81$), soil in warmer sites did have the largest concentrations of FeOx ($F_{1,46} = 11.75$; $p = 0.001$). However, this pattern does not seem to have resulted in a confounding effect of climate on MAOM C concentrations: despite warmer sites having overall higher concentrations of FeOx, the concentration of MAOM C was lower in these sites. Therefore, we suggest that climate-driven variation in SOM C concentrations in our study is not likely due to covarying effects of climate on soil mineralogy or organic matter production.

4.4 | Carbon isotopes and mineral-associated organic matter decomposition and persistence

During microbial respiration, physical fractionation of heavy and light carbon molecules generally favours the loss of lighter (i.e. ^{12}C) carbon as carbon dioxide gas, while heavier ^{13}C and ^{14}C are incorporated into microbial biomass. Therefore, we expected MAOM carbon in warmer sites to have more enriched $\delta^{13}C$ and $\Delta^{14}C$ signatures due to the generally faster rates of microbial decomposition and C cycling with increasing mean annual temperature (Shi et al., 2020; Yang et al., 2014). Instead, we found a minor decrease in $\delta^{13}C$ with increasing CDI, and no effect of CDI on $\Delta^{14}C$ (Table 4; Figure S3). Furthermore, $\delta^{13}C$ increased with the percentage of FeOx in our samples, although this trend was most evident at LENO, where the largest variation in FeOx was observed (Figure S3). Given the positive association between concentrations of MAOM C and N and FeOx, this pattern in $\delta^{13}C$ may be due to overall faster rates of microbial activity and opportunity for organo-mineral interactions at this site, where both climate and mineralogy are well suited for MAOM formation. As has been noted in other studies, soil radiocarbon content across our study sites were not necessarily correlated with the

factors that controlled the concentrations of C and N in SOM fractions (Heckman, Nave, et al., 2021; McFarlane et al., 2013).

These patterns suggest that local conditions, perhaps land use history, hydrology, or soil disturbance, may be more important than climate, microbial communities or the availability of potential binding sites for explaining variation in MAOM turnover times within biomes. For example, the lowest $\Delta^{14}C$ values, indicating older MAOM C, were measured at DELA, a seasonally flooded bottomland forest, where, despite a high mean annual temperature, soil inundation likely limits decomposition and supports the persistence of MAOM C, while inhibiting the formation of new MAOM. Conversely, the high $\Delta^{14}C$ values at SERC may be due to the regular mixing of new litter material into the mineral soil by the invasive earthworm *Lumbricus rubellus* (Crow et al., 2009). The radiocarbon content of the MAOM at other sites in our study was relatively consistent, with most C reflecting a near-modern origin, despite variation in climate and soil type. Although others have identified broad-scale patterns in soil $\Delta^{14}C$ corresponding with climate and soil mineralogy (Mathieu et al., 2015; Shi et al., 2020), it is likely that the variation in these factors among the sites used in our study was insufficient to demonstrate these effects.

The site-specific conditions that may have influenced MAOM carbon age in our study may be difficult to identify in broad-scale analyses of soil carbon age. Therefore, to accurately predict fine-scale variation in MAOM persistence, we suggest that individually derived models of MAOM turnover based on local conditions that influence SOM decomposition rates are needed. Additionally, it is generally accepted that MAOM pools are heterogeneous in nature, with fast-cycling and slow-cycling components that are governed by distinct environmental conditions and inputs and likely vary in their chemical compositions (Neurath et al., 2021; Sokol et al., 2022). Therefore, it is possible that drivers of MAOM C and N concentrations in our sites also exert important controls on MAOM persistence in either the slow-cycling or fast-cycling fraction but that these patterns were not detectable in our analysis of MAOM radiocarbon content. Furthermore, because radiocarbon-based estimates of MAOM age represent the average persistence of both fast and slow-cycling MAOM fractions, the patterns observed here do not necessarily reflect the stability of the total MAOM pool across our study sites, but rather offer a general comparison of the average MAOM C turnover time.

5 | CONCLUSIONS

We show that soil reactive iron content was the best predictor of MAOM C and N concentrations in the upper mineral soils in eastern US forests but that tree mycorrhizal type influenced the relative proportion of C in POM versus MAOM and the C:N of both POM and MAOM. Specifically, in forests dominated by AM-associated trees, we found that a higher proportion of the soil C was stored in the MAOM versus the POM fraction and that the MAOM in these forests generally had a lower C:N. Additionally, we identified a trend suggesting that climate may influence the effect of tree mycorrhizal type on the MAOM N concentrations and the proportion of N in MAOM: forests dominated by ECM-associated trees stored relatively more soil N as MAOM in colder climates, but less soil N as MAOM in warmer climates, when compared with stands dominated by AM-associated trees. Radiocarbon content of the mineral-associated soil fraction did not help explain potential mechanisms for the patterns we found in MAOM C and N concentrations. Instead, the MAOM fraction radiocarbon age was unrelated to soil mineralogy, tree mycorrhizal type, or climate, suggesting that other factors operating at local scales may be more important for explaining variation in MAOM turnover within biomes. These results support recent findings that mycorrhizal fungi influence the distribution of soil C and N among different SOM fractions, which vary in their vulnerability to decay and are thus critical for predicting soil C and N dynamics in a changing climate. Given the potential interactive effects of climate and tree mycorrhizal type on the proportion of soil N in MAOM versus POM, we encourage models of the controls on SOM C and N pools across large spatial scales to more directly account for how the primary drivers of MAOM and POM pools may vary across climate gradients.

AUTHOR CONTRIBUTIONS

Ashley K. Lang, Rich Phillips and Jennifer Pett-Ridge conceived of and designed the study, Rich Phillips, Karis J. McFarlane and Jennifer Pett-Ridge provided institutional support for analyses, Ashley K. Lang and Karis J. McFarlane conducted laboratory analyses, Ashley K. Lang wrote the manuscript, and all authors contributed substantially to edits and improvements.

ACKNOWLEDGEMENTS

The National Ecological Observatory Network is a program sponsored by the National Science Foundation and operated under a cooperative agreement by Battelle. This material uses samples collected as part of the NEON Program. The authors thank Kelsey Yule for assisting with the selection and acquisition of soil samples needed to conduct this work. We further thank Elizabeth Huenupi-Pena for assistance with laboratory analyses. This work was supported by a National Science Foundation Postdoctoral Research Fellowship in Biology awarded to A.K.L (2010724). Work at Lawrence Livermore National Laboratory (LLNL) was supported by the U.S. Department of Energy (DOE), Office of Biological and Environmental Research (BER), Genomic Science Program, LLNL 'Microbes Persist' Soil Microbiome Scientific Focus Area SCW1632, under the auspices of the DOE, Contract DE-AC52-07NA27344.

CONFLICT OF INTEREST STATEMENT

The authors declare no conflict of interest.

PEER REVIEW

The peer review history for this article is available at https://www.webofscience.com/api/gateway/wos/peer-review/10.1111/1365-2745.14094.

DATA AVAILABILITY STATEMENT

Woody vegetation data (DP1.10098.001) and leaf litter production and chemistry data (DP1.10033.001) for the NEON sites used in this study are available on the NEON Data Portal (https://data.neonscience.org/). Other data and code for the analyses generated by this work are archived via Zenodo at: https://doi.org/10.5281/zenodo.7699916 (Lang, 2023).

ORCID

Ashley K. Lang https://orcid.org/0000-0002-6080-1681
Jennifer Pett-Ridge https://orcid.org/0000-0002-4439-2398
Karis J. McFarlane https://orcid.org/0000-0001-6390-7863
Richard P. Phillips https://orcid.org/0000-0002-1345-4138

REFERENCES

Adair, E. C., Parton, W. J., del Grosso, S. J., Silver, W. L., Harmon, M. E., Hall, S. A., Burke, I. C., & Hart, S. C. (2008). Simple three-Pool model accurately describes patterns of long-term litter decomposition in diverse climates. *Global Change Biology*, *14*(11), 2636–2660.

Amelung, W., Bossio, D., de Vries, W., Kögel-Knabner, I., Lehmann, J., Amundson, R., Bol, R., Collins, C., Lal, R., Leifeld, J., Minasny, B., Pan, G., Paustian, K., Rumpel, C., Sanderman, J., van Groenigen, J. W., Mooney, S., van Wesemael, B., Wander, M., & Chabbi, A. (2020). Towards a global-scale soil climate mitigation strategy. *Nature Communications*, *11*(1), 1–10.

Angst, G., Mueller, K. E., Nierop, K. G. J., & Simpson, M. J. (2021). Plant- or microbial-derived? A review on the molecular composition of stabilized soil organic matter. *Soil Biology & Biochemistry*, *156*(May), 108189.

Bates, D., Mächler, M., Bolker, B., & Walker, S. (2015). Fitting linear mixed-effects models using lme4. *Journal of Statistical Software*, *67*(1), 1–48.

Bossio, D. A., Cook-Patton, S. C., Ellis, P. W., Fargione, J., Sanderman, J., Smith, P., Wood, S., Zomer, R. J., von Unger, M., Emmer, I. M., & Griscom, B. W. (2020). The role of soil carbon in natural climate solutions. *Nature Sustainability*, *3*(5), 391–398.

Broek, T. A. B., Ognibene, T. J., McFarlane, K. J., Moreland, K. C., Brown, T. A., & Bench, G. (2021). Conversion of the LLNL/CAMS 1 MV biomedical AMS system to a semi-automated natural abundance ^{14}C spectrometer: System optimization and performance evaluation. *Nuclear Instruments & Methods in Physics Research. Section B, Beam Interactions with Materials and Atoms*, *499*(July), 124–132.

Carteron, A., Beigas, M., Joly, S., Turner, B. L., & Laliberté, E. (2020). Temperate forests dominated by Arbuscular or ectomycorrhizal fungi are characterized by strong shifts from saprotrophic to Mycorrhizal fungi with increasing soil depth. *Microbial Ecology*, *82*, 377–390. https://doi.org/10.1007/s00248-020-01540-7

Catford, J. A., Wilson, J. R. U., Pyšek, P., Hulme, P. E., & Duncan, R. P. (2022). Addressing context dependence in ecology. *Trends in Ecology & Evolution*, *37*(2), 158–170.

Cheeke, T. E., Phillips, R. P., Brzostek, E. R., Rosling, A., Bever, J. D., & Fransson, P. (2016). Dominant mycorrhizal association of trees alters carbon and nutrient cycling by selecting for microbial groups with distinct enzyme function. *The New Phytologist*, *214*(1), 432–442.

Cornelissen, J., Aerts, R., Cerabolini, B., Werger, M., & van der Heijden, M. (2001). Carbon cycling traits of plant species are linked with Mycorrhizal strategy. *Oecologia*, *129*(4), 611–619.

Cotrufo, M. F., Ranalli, M. G., Haddix, M. L., Six, J., & Lugato, E. (2019). Soil carbon storage informed by particulate and mineral-associated organic matter. *Nature Geoscience*, *12*(12), 989–994.

Cotrufo, M. F., Wallenstein, M. D., Boot, C. M., Denef, K., & Paul, E. (2013). The microbial efficiency-matrix stabilization (MEMS) framework integrates plant litter decomposition with soil organic matter stabilization: Do labile plant inputs form stable soil organic matter? *Global Change Biology*, *19*(4), 988–995.

Craig, M. E., Geyer, K. M., Beidler, K. V., Brzostek, E. R., Frey, S. D., Stuart Grandy, A., Liang, C., & Phillips, R. P. (2022). Fast-decaying plant litter enhances soil carbon in temperate forests but not through microbial physiological traits. *Nature Communications*, *13*(1), 1229.

Craig, M. E., Turner, B. L., Liang, C., Clay, K., Johnson, D. J., & Phillips, R. P. (2018). Tree Mycorrhizal type predicts within-site variability in the storage and distribution of soil organic matter. *Global Change Biology*, *24*(8), 3317–3330.

Crow, S. E., Lajtha, K., Filley, T. R., Swanston, C. W., Bowden, R. D., & Caldwell, B. A. (2009). Sources of plant-derived carbon and stability of organic matter in soil: Implications for global change. *Global Change Biology*, *15*(8), 2003–2019.

Fernandez, C. W., Adam Langley, J., Samantha Chapman, M., McCormack, L., & Koide, R. T. (2016). The decomposition of ectomycorrhizal fungal Necromass. *Soil Biology & Biochemistry*, *93*, 38–49.

Fitch, A. A., Lang, A., Whalen, E., & Geyer, K. M. (2020). Fungal community, not substrate quality, drives soil microbial function in northeast temperate forests. *Frontiers in Forests and Global Change*, *3*. https://doi.org/10.3389/ffgc.2020.569945

Fossum, C., Estera-Molina, K. Y., Yuan, M., Herman, D. J., Chu-Jacoby, I., Nico, P. S., Morrison, K. D., Pett-Ridge, J., & Firestone, M. K. (2022). Belowground allocation and dynamics of recently fixed plant carbon in a California annual grassland. *Soil Biology & Biochemistry*, *165*(February), 108519.

Frey, S. D. (2019). Mycorrhizal fungi as mediators of soil organic matter dynamics. *Annual Review of Ecology, Evolution, and Systematics*, *50*(1), 237–259.

Haddix, M. L., Gregorich, E. G., Helgason, B. L., Janzen, H., Ellert, B. H., & Francesca Cotrufo, M. (2020). Climate, carbon content, and soil texture control the independent formation and persistence of particulate and mineral-associated organic matter in soil. *Geoderma*, *363*(April), 114160.

Hakkenberg, C. R., Goetz, S. J., & Gillespie, T. (2021). Climate mediates the relationship between plant biodiversity and Forest structure across the United States. *Global Ecology and Biogeography: A Journal of Macroecology*, *30*(11), 2245–2258.

Heckman, K. A., Lawrence, C. R., Harden, J. W., Crate, J., & Swanston, C. (2015). *Ironing out the details of soil organic matter cycling: The unique role of Fe-bearing minerals in regulating organic matter transformation in soils*. B32C-01.

Heckman, K. A., Nave, L. E., Bowman, M., Gallo, A., Hatten, J. A., Matosziuk, L. M., Possinger, A. R., SanClements, M., Strahm, B. D., Weiglein, T. L., Rasmussen, C., & Swanston, C. W. (2021). Divergent controls on carbon concentration and persistence between forests and grasslands of the conterminous US. *Biogeochemistry*, *156*(1), 41–56.

Heckman, K. A., Swanston, C. W., Torn, M. S., Hanson, P. J., Nave, L. E., Porras, R. C., Mishra, U., & Bill, M. (2021). Soil organic matter is principally root derived in an Ultisol under oak Forest. *Geoderma*, *403*(December), 115385.

Heckman, K., Hicks, C. E., Pries, C. R., Lawrence, C. R., Crow, S. E., Hoyt, A. M., von Fromm, S. F., Shi, Z., Stoner, S., McGrath, C., Beem-Miller, J., Berhe, A. A., Blankinship, J. C., Keiluweit, M., Marín-Spiotta, E., Monroe, J. G., Plante, A. F., Schimel, J., Sierra, C. A., … Wagai, R. (2022). Beyond bulk: Density fractions explain heterogeneity in global soil carbon abundance and persistence. *Global Change Biology*, *28*(3), 1178–1196. https://doi.org/10.1111/gcb.16023

Heckman, K., Lawrence, C. R., & Harden, J. W. (2018). A sequential selective dissolution method to quantify storage and stability of organic

carbon associated with Al and Fe hydroxide phases. *Geoderma*, *312*(February), 24–35.
Hinckley, E.-L. S., Bonan, G. B., Bowen, G. J., Colman, B. P., Duffy, P. A., Goodale, C. L., Houlton, B. Z., Marín-Spiotta, E., Ogle, K., Ollinger, S. V., Paul, E. A., Vitousek, P. M., Weathers, K. C., & Williams, D. G. (2016). The soil and plant biogeochemistry sampling Design for the National Ecological Observatory Network. *Ecosphere*, *7*(3), e01234. https://doi.org/10.1002/ecs2.1234
Hoffland, E., Kuyper, T. W., Comans, R. N. J., & Creamer, R. E. (2020). Eco-functionality of organic matter in soils. *Plant and Soil*, *455*(1), 1–22.
Huang, W., van Bodegom, P. M., Declerck, S., Heinonsalo, J., Cosme, M., Viskari, T., Liski, J., & Soudzilovskaia, N. A. (2022). Mycelium chemistry differs markedly between ectomycorrhizal and Arbuscular Mycorrhizal fungi. *Communications Biology*, *5*(1), 398.
Jevon, F. V., & Lang, A. K. (2022). Tree biomass allocation differs by Mycorrhizal association. *Ecology*, *103*(6), e3688.
Jilling, A., Keiluweit, M., Contosta, A. R., Frey, S., Schimel, J., Schnecker, J., Smith, R. G., Tiemann, L., & Stuart Grandy, A. (2018). Minerals in the rhizosphere: Overlooked mediators of soil nitrogen availability to Plants and microbes. *Biogeochemistry*, *139*(2), 103–122.
Jilling, A., Keiluweit, M., Gutknecht, J. L. M., & Stuart Grandy, A. (2021). Priming mechanisms providing Plants and microbes access to mineral-associated organic matter. *Soil Biology & Biochemistry*, *158*, 108265.
Jones, A. R., Sanderman, J., Allen, D., Dalal, R., & Schmidt, S. (2015). Subtropical giant podzol chronosequence reveals that soil carbon stabilisation is not governed by litter quality. *Biogeochemistry*, *124*(1), 205–217.
Keiluweit, M., Bougoure, J. J., Nico, P. S., Pett-Ridge, J., Weber, P. K., & Kleber, M. (2015). Mineral protection of soil carbon counteracted by root exudates. *Nature Climate Change*, *5*(6), 588–595.
Keiluweit, M., Bougoure, J. J., Zeglin, L. H., Myrold, D. D., Weber, P. K., Pett-Ridge, J., Kleber, M., & Nico, P. S. (2012). Nano-scale investigation of the association of microbial nitrogen residues with iron (hydr)oxides in a forest soil O-horizon. *Geochimica et Cosmochimica Acta*, *95*(October), 213–226.
Keller, A. B., Brzostek, E. R., Craig, M. E., Fisher, J. B., & Phillips, R. P. (2021). Root-derived inputs are major contributors to soil carbon in temperate forests, but vary by Mycorrhizal type. *Ecology Letters*, *24*(4), 626–635.
Keller, A. B., & Phillips, R. P. (2019). Leaf litter decay rates differ between Mycorrhizal groups in temperate, but not tropical, forests. *The New Phytologist*, *222*(1), 556–564.
Kleber, M., Mikutta, R., Torn, M. S., & Jahn, R. (2005). Poorly crystalline mineral phases protect organic matter in acid subsoil horizons. *European Journal of Soil Science*, *56*, 717–725. https://doi.org/10.1111/j.1365-2389.2005.00706.x
Kögel-Knabner, I., Guggenberger, G., Kleber, M., Kandeler, E., Kalbitz, K., Scheu, S., Eusterhues, K., & Leinweber, P. (2008). Organo-mineral associations in temperate soils: Integrating biology, mineralogy, and organic matter chemistry. *Journal of Plant Nutrition and Soil Science*, *171*(1), 61–82.
Kramer, M. G., & Chadwick, O. A. (2018). Climate-driven thresholds in reactive mineral retention of soil carbon at the global scale. *Nature Climate Change*, *8*, 1104–1108.
Lal, R. (2004). Soil carbon sequestration impacts on global climate change and food security. *Science*, *304*(5677), 1623–1627.
Lambers, H., Raven, J. A., Shaver, G. R., & Smith, S. E. (2008). Plant nutrient-acquisition strategies change with soil age. *Trends in Ecology & Evolution*, *23*(2), 95–103.
Lang, A. (2023). Ashleylang/NEON_MAOM: MAOM C and N in NEON forests of the eastern U.S. V.01 march 2023 (v.01). *Zenodo*, https://doi.org/10.5281/zenodo.7699916
Lehmann, J., & Kleber, M. (2015). The contentious nature of soil organic matter. *Nature*, *528*, 60–68. https://doi.org/10.1038/nature16069
Liang, C., Amelung, W., Lehmann, J., & Kästner, M. (2019). Quantitative assessment of microbial Necromass contribution to soil organic matter. *Global Change Biology*, *25*(11), 3578–3590.
Lloyd, J., & Taylor, J. A. (1994). On the temperature dependence of soil respiration. *Functional Ecology*, *8*(3), 315–323.
Lovett, G. M., Goodale, C. L., & Ollinger, S. V. (2018). Nutrient retention during ecosystem succession: A revised conceptual model. *Frontiers in Ecology and the Environment*, *16*(9), 532–538.
Lugato, E., Lavallee, J. M., Haddix, M. L., Panagos, P., & Francesca Cotrufo, M. (2021). Different climate sensitivity of particulate and mineral-associated soil organic matter. *Nature Geoscience*, *14*(5), 295–300.
Lunch, C., Laney, C., Mietkiewicz, N., Sokol, E., Cawley, K., & NEON (National Ecological Observatory Network). (2021). *neonUtilities: Utilities for working with NEON data*. https://CRAN.R-project.org/package=neonUtilities
Mathieu, J. A., Hatté, C., Balesdent, J., & Parent, É. (2015). Deep soil carbon dynamics are driven more by soil type than by climate: A worldwide meta-analysis of radiocarbon profiles. *Global Change Biology*, *21*(11), 4278–4292.
McFarlane, K. J., Torn, M. S., Hanson, P. J., Porras, R. C., Swanston, C. W., Callaham Jr, M. A., & Guilderson, T. P. (2013). Comparison of soil organic matter dynamics at five temperate deciduous forests with physical fractionation and radiocarbon measurements. *Biogeochemistry*, *112*(1–3), 457–476.
Mikutta, R., Kleber, M., Torn, M. S., & Jahn, R. (2006). Stabilization of soil organic matter: Association with minerals or chemical recalcitrance? *Biogeochemistry*, *77*(1), 25–56.
Mikutta, R., Turner, S., Schippers, A., Gentsch, N., Meyer-Stüve, S., Condron, L. M., Peltzer, D. A., Richardson, S. J., Eger, A., Hempel, G., Kaiser, K., Klotzbücher, T., & Guggenberger, G. (2019). Microbial and abiotic controls on mineral-associated organic matter in soil profiles along an ecosystem gradient. *Scientific Reports*, *9*(1), 10294.
Moore, J. A. M., Jiang, J., Patterson, C. M., Mayes, M. A., Wang, G., & Classen, A. T. (2015). Interactions among roots, mycorrhizas and free-living microbial communities differentially impact soil carbon processes. *The Journal of Ecology*, *103*(6), 1442–1453. https://doi.org/10.1111/1365-2745.12484
Nave, L. E., Bowman, M., Gallo, A., Hatten, J. A., Heckman, K. A., Matosziuk, L., Possinger, A. R., SanClements, M., Sanderman, J., Strahm, B. D., Weiglein, T. L., & Swanston, C. W. (2021). Patterns and predictors of soil organic carbon storage across a continental-scale network. *Biogeochemistry*, *156*(1), 75–96.
NEON. (2022a). *Litterfall and fine woody debris production and chemistry*. (DP1.10033.001). National Ecological Observatory Network. https://doi.org/10.48443/b2qt-7z79
NEON. (2022b). *Vegetation structure* (DP1.10098.001). National Ecological Observatory Network. https://doi.org/10.48443/RE8N-TN87
Neurath, R. A., Pett-Ridge, J., Chu-Jacoby, I., Herman, D., Whitman, T., Nico, P. S., Lipton, A. S., Kyle, J., Tfaily, M. M., Thompson, A., & Firestone, M. K. (2021). Root carbon interaction with soil minerals is dynamic, leaving a legacy of Microbially derived residues. *Environmental Science & Technology*, *55*(19), 13345–13355.
Paustian, K., Larson, E., Kent, J., Marx, E., & Swan, A. (2019). Soil C sequestration as a biological negative emission strategy. *Frontiers in Climate*, *1*(October). https://doi.org/10.3389/fclim.2019.00008
Pellitier, P. T., & Zak, D. R. (2018). Ectomycorrhizal fungi and the enzymatic liberation of nitrogen from soil organic matter: Why evolutionary history matters. *The New Phytologist*, *217*(1), 68–73.
PRISM Climate Group, Oregon State University. (n.d.). *Parameter-Elevation Regressions on Independent Slopes Model (PRISM) Dataset*. www.prism.oregonstate.edu
Rasmussen, C., Heckman, K., Wieder, W. R., Keiluweit, M., Lawrence, C. R., Berhe, A. A., Blankinship, J. C., Crow, S. E., Druhan, J. L., Hicks Pries, C. E., Marin-Spiotta, E., Plante, A. F., Schädel, C., Schimel, J. P., Sierra, C. A., Thompson, A., & Wagai, R. (2018). Beyond Clay: Towards an improved set of variables for predicting soil organic matter content. *Biogeochemistry*, *137*(3), 297–306.

Scharlemann, J. P. W., Tanner, E. V. J., Hiederer, R., & Kapos, V. (2014). Global soil carbon: Understanding and managing the largest terrestrial carbon Pool. *Carbon Management*, *5*(1), 81–91.

Schöning, I., Knicker, H., & Kögel-Knabner, I. (2005). Intimate association between O/N-alkyl carbon and iron oxides in Clay fractions of Forest soils. *Organic Geochemistry*, *36*(10), 1378–1390.

Shi, Z., Allison, S. D., He, Y., Levine, P. A., Hoyt, A. M., Beem-Miller, J., Zhu, Q., Wieder, W. R., Trumbore, S., & Randerson, J. T. (2020). The age distribution of global soil carbon inferred from radiocarbon measurements. *Nature Geoscience*, *13*(8), 555–559.

Singavarapu, B., Beugnon, R., Bruelheide, H., Cesarz, S., Jianqing, D., Eisenhauer, N., Guo, L.-D., Nawaz, A., Wang, Y., Xue, K., & Wubet, T. (2022). Tree mycorrhizal type and tree diversity shape the Forest soil microbiota. *Environmental Microbiology*, *24*(9), 4236–4255. https://doi.org/10.1111/1462-2920.15690

Slessarev, E. W., Chadwick, O. A., Sokol, N. W., Nuccio, E. E., & Pett-Ridge, J. (2022). Rock weathering controls the potential for soil carbon storage at a continental scale. *Biogeochemistry*, *157*(1), 1–13.

Sokol, N. W., Sanderman, J., & Bradford, M. A. (2018). Pathways of mineral-associated soil organic matter formation: Integrating the role of plant carbon source, chemistry, and point of entry. *Global Change Biology*, *25*(1), 12–24.

Sokol, N. W., Whalen, E. D., Jilling, A., Kallenbach, C., Pett-Ridge, J., & Georgiou, K. (2022). Global distribution, formation and fate of mineral-associated soil organic matter under a changing climate: A trait-based perspective. *Functional Ecology*, *36*, 1411–1429. https://doi.org/10.1111/1365-2435.14040

Sollins, P., Kramer, M. G., Swanston, C., Lajtha, K., Filley, T., Aufdenkampe, A. K., Wagai, R., & Bowden, R. D. (2009). Sequential density fractionation across soils of contrasting mineralogy: Evidence for both microbial- and mineral-controlled soil organic matter stabilization. *Biogeochemistry*, *96*(1), 209–231.

Soranno, P. A., Cheruvelil, K. S., Bissell, E. G., Bremigan, M. T., Downing, J. A., Fergus, C. E., Filstrup, C. T., Henry, E. N., Lottig, N. R., Stanley, E. H., Stow, C. A., Tan, P.-N., Wagner, T., & Webster, K. E. (2014). Cross-scale interactions: Quantifying multi-scaled cause–effect relationships in macrosystems. *Frontiers in Ecology and the Environment*, *12*(1), 65–73.

Stuiver, M., & Polach, H. A. (1977). Discussion reporting of ^{14}C data. *Radiocarbon*, *19*(3), 355–363.

Swanston, C. W., Torn, M. S., Hanson, P. J., Southon, J. R., Garten, C. T., Hanlon, E. M., & Ganio, L. (2005). Initial characterization of processes of soil carbon stabilization using Forest stand-level radiocarbon enrichment. *Geoderma*, *128*(1), 52–62.

Swenson, T. L., Bowen, B. P., Nico, P. S., & Northen, T. R. (2015). Competitive sorption of microbial metabolites on an iron oxide mineral. *Soil Biology & Biochemistry*, *90*(November), 34–41.

Tedersoo, L., & Bahram, M. (2019). Mycorrhizal types differ in ecophysiology and Alter Plant nutrition and soil processes. *Biological Reviews of the Cambridge Philosophical Society*, *94*(5), 1857–1880.

Tedersoo, L., Bahram, M., Cajthaml, T., Põlme, S., Hiiesalu, I., Anslan, S., Harend, H., Buegger, F., Pritsch, K., Koricheva, J., & Abarenkov, K. (2016). Tree diversity and species identity effects on soil fungi, Protists and animals are context dependent. *The ISME Journal*, *10*(2), 346–362.

Torn, M. S., Trumbore, S. E., Chadwick, O. A., Vitousek, P. M., & Hendricks, D. M. (1997). Mineral control of soil organic carbon storage and turnover. *Nature*, *389*(6647), 170–173.

Trumbore, S., Gaudinski, J. B., Hanson, P. J., & Southon, J. R. (2002). Quantifying ecosystem-atmosphere carbon exchange with a ^{14}C label. *Eos*, *83*(24), 265.

USDA, NRCS. National Plant Data Team. (2021). *The PLANTS Database*. http://plants.usda.gov

Vogel, J. S., Southon, J. R., Nelson, D. E., & Brown, T. A. (1984). Performance of catalytically condensed carbon for use in accelerator mass-spectrometry. *Nuclear Instruments and Methods in Physics Research Section B: Beam Interactions with Materials and Atoms*, *5*(2), 289–293.

Waring, B. G., Sulman, B. N., Sasha Reed, A., Smith, P., Averill, C., Creamer, C. A., Cusack, D. F., Hall, S. J., Jastrow, J. D., Jilling, A., Kemner, K. M., Kleber, M., Liu, X.-J. A., Pett-Ridge, J., & Schulz, M. (2020). From pools to flow: The PROMISE framework for new insights on soil carbon cycling in a changing world. *Global Change Biology*, *26*(12), 6631–6643. https://doi.org/10.1111/gcb.15365

Weng, Y.-T., Wang, C.-C., Chiang, C.-C., Tsai, H., Song, Y.-F., Huang, S.-T., & Liang, B. (2018). In situ evidence of mineral physical protection and carbon stabilization revealed by nanoscale 3-D tomography. *Biogeosciences*, *15*(10), 3133–3142.

Yang, W., Magid, J., Christensen, S., Rønn, R., Ambus, P., & Ekelund, F. (2014). Biological ^{12}C–^{13}C fractionation increases with increasing community-complexity in soil microcosms. *Soil Biology & Biochemistry*, *69*(February), 197–201.

Yu, W., Huang, W., Weintraub-Leff, S. R., & Hall, S. J. (2022). Where and why do particulate organic matter (POM) and mineral-associated organic matter (MAOM) differ among diverse soils? *Soil Biology & Biochemistry*, *172*(September), 108756.

SUPPORTING INFORMATION

Additional supporting information can be found online in the Supporting Information section at the end of this article.

Table S1: Proportions of tree basal area in each study plot from species associated with AM fungi, ECM fungi, and ericoid mycorrhizal (ERM) fungi.

Table S2: Random effects of Site from models presented in Table 2: the concentrations and proportions of C and N in MAOM from plots located within seven forests in the National Ecological Observatory Network (NEON).

Table S3: Random effects of Site from models presented in Table 3: C:N in fPOM, oPOM, and MAOM from plots located within seven forests in the National Ecological Observatory Network (NEON).

Table S4: Random effects of Site from models presented in Table 4: MAOM $\delta^{13}C$ and $\Delta^{14}C$ from plots located within seven forests in the National Ecological Observatory Network (NEON).

Figure S1: Proportions of total soil N in the (a) free particulate fraction (N_{fPOM}), (b) occluded particulate fraction (N_{oPOM}) and (c) mineral-associated organic matter (N_{MAOM}) fraction in plots situated along a gradient of tree mycorrhizal dominance in seven forested NEON sites (see Table 1 for site definitions). Points represent individual plots within each study site ($n = 46$). Lines reflect the best fit from linear models specific to each study site.

Figure S2: Mean annual litterfall collected per sampling trap area within forest plots in seven National Ecological Observatory Network (NEON) sites. Annual masses of leaf and needle litter falling within each plot were averaged for the years with available and complete litterfall data, which varied by site and ranged from 2016 to 2019. Litterfall mass is plotted against the relative percentage of tree basal area represented by tree species with known associations with ectomycorrhizal (ECM) fungi. Solid lines indicate significant relationships at $\alpha = 0.05$.

Figure S3: Trends in mineral-associated organic matter carbon isotope ratios with climate decomposition index (CDI), % ECM tree basal area and oxalate-extractable iron content from soil samples collected within six forests in the National Ecological Observatory Network (NEON). Solid lines indicate significant linear relationships at $\alpha = 0.05$. See Table 4 and Table S4 for the results of the statistical models.

How to cite this article: Lang, A. K., Pett-Ridge, J., McFarlane, K. J., & Phillips, R. P. (2023). Climate, soil mineralogy and mycorrhizal fungi influence soil organic matter fractions in eastern US temperate forests. *Journal of Ecology*, *111*, 1254–1269. https://doi.org/10.1111/1365-2745.14094